JOURNAL OF AGRICULTURAL AND FOOD CHEMISTRY

pubs.acs.org/JAFC Article

# Structural and Functional Characterization of European Corn Borer, *Ostrinia nubilalis*, Pheromone Binding Protein 3

Omar Al-Danoon, Suman Mazumder, Bharat P. Chaudhary, Viswanath Nukala, Benton Bishop, Gage Cahoon, and Smita Mohanty*

Cite This: https://doi.org/10.1021/acs.jafc.1c03775 Read Online

ACCESS | Metrics & More | Article Recommendations | Supporting Information

**ABSTRACT:** *Ostrinia nubilalis*, a lepidopteran moth, also known as the European corn borer, has a major impact on the production of economically important crops in the United States and Europe. The female moth invites the male moth for mating through the release of pheromones, a volatile chemical signal. Pheromone binding proteins (PBPs) present in the male moth antennae are believed to pick up the pheromones, transport them across the aqueous sensillum lymph, and deliver them to the olfactory receptor neurons. Here we report for the first time the cloning, expression, refolding, purification, and structural characterization of *Ostrinia nubilalis* PBP3 (OnubPBP3). The recombinant protein showed nanomolar affinity to each isomer of the *Ostrinia* pheromones, E- and Z-11-tetradecenyl acetate. In a pH titration study by nuclear magnetic resonance, the protein exhibited an acid-induced unfolding at pH below 5.5. The molecular dynamics simulation study demonstrated ligand-induced conformational changes in the protein with both E- and Z-isomers of the *Ostrinia* pheromone. The simulation studies showed that while protein flexibility decreases upon binding to E-pheromone, it increases when bound to Z-pheromone. This finding suggests that the OnubPBP3 complex with E-pheromone is more stable than with Z-pheromone.

**KEYWORDS:** *pheromone binding proteins, Ostrinia nubilalis, NMR, molecular dynamics simulation, fluorescence spectroscopy, ligand binding, OnubPBP3*



## INTRODUCTION

Chemoreception is an essential process for the regulation of insect behaviors such as mating, feeding, oviposition, and predator avoidance. Chemoreception allows insects to detect various olfactory stimuli (semiochemicals) that translate into nerve impulses influencing insect behavior. Diverse proteins are involved in the signaling process of the chemical stimuli, including odorant binding proteins (OBPs), chemosensory proteins, odorant receptors, and sensory neuron membrane proteins. Pheromone binding proteins (PBPs) are a class of OBPs that specifically transport sex pheromones to the olfactory receptor neuron.[1] PBPs are acidic and water-soluble with a molecular mass of 14−16 kDa. Sex pheromones are small volatile hydrophobic molecules produced and emitted by female insects to trigger the mating behavior in males. Male insects, especially lepidopteran moths, receive the chemical message through a relatively large antenna where pheromone receptors are surrounded by an aqueous solution, the sensillar lymph. To reach the receptors, the hydrophobic pheromone molecules are ferried across the aqueous lymph while being protected from degrading enzymes by the PBPs that encapsulate them in their hydrophobic binding pockets.[2−4]

The European corn borer, *Ostrinia nubilalis* (Lepidoptera: Crambidae), an invasive pest, damages a variety of crops especially corn, a major grain of economic importance. The insect first appeared in the United States in 1917. *O. nubilalis* has disseminated massively throughout the nation, in particular the northeastern part of the USA. An annual loss of over $1 billion from reduced crop yield has been estimated because of the damage caused by *O. nubilalis* in the United States.[5,6] In addition to North America, *Ostrinia* is a major insect pest in other parts of the world, including Europe and Central Asia. A sister species, *O. furnacalis*, is a common agricultural pest in Asia and Oceania. Despite the fact that both *O. nubilalis* and *O. furnacalis* belong to the same subgroup, called trilobed uncus, their males respond to distinct sex pheromones.[7] Odorant receptors of *O. nubilalis* males are stimulated via a blend of E- and Z-isomers of 11-tetradecenyl-acetate (E/Z-11-14:OAc) (Figure 1).[8,9] On the other hand, a blend of E- and Z-isomers of 12-tetradecenyl-acetate (E/Z-12-14:OAc) stimulates the odorant receptors of *O. furnacalis* males.[10] Pheromone polymorphism has been reported for *O. nubilalis* with regard to the ratio of the pheromone blend.[11] Some females produce an E:Z blend with a ratio equal to 99:1 and some others produce the blend with a ratio of 3:97.[12,13] Based on the ratio of the pheromone blend, the response of *O. nubilalis* males differ.[11] Thus, *O. nubilalis* can be classified into two strains: E- and Z-strain. Males of the E-strain are attracted to a blend with 99% E-pheromone while males of the Z-strain are attracted to the other blend with 97% Z-pheromone.[9,11,14,15] Although the males of E- and Z-strains respond to a specific pheromone

Received: June 30, 2021
Revised: October 28, 2021
Accepted: November 1, 2021

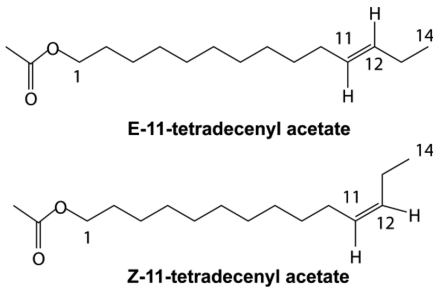


**Figure 1.** Chemical structures of *Ostrinia nubilalis* pheromones.

blend, there are no differences in the primary structure of their PBPs. Based on this observation, it has been suggested that PBPs are not directly responsible for the recognition between the strains.[16] Five distinguishable PBPs have been reported to be present in the male antennae of *O. nubilalis* species: PBP1, PBP2, PBP3, PBP4, and PBP5.[17] Neither the binding affinities to the pheromones nor the mechanisms of pheromone binding and release are known. PBP2 and PBP3 are expressed at higher levels in the antennae of males than in the females. Based on protein-sequence comparisons between the PBPs of *O. nubilalis* and *O. furnacalis*, it appears that PBP3 plays a key role in pheromone selection as their sequences differ the most.[17]

The male-biased OnubPBP3 has over 50% sequence identity to other well-studied lepidopteran PBPs from *Antheraea polyphemus* (ApolPBP1),[18−24] *Amyelois transitella* (AtraPBP1),[25,26] *Bombyx mori* (BmorPBP),[27−34] and *Lymantria dispar* (LdisPBPs)[35,36] (Figure 2). OnubPBP3 containing 144 residues has a calculated molecular mass of 16.3 kDa with a pI of 5.28 suggesting that this is a small acidic protein. It also contains six conserved cysteine residues that may form disulfide bonds to stabilize the helices that form a hydrophobic pocket in the interior of the protein, similar to other PBPs. However, unlike the PBPs shown in Figure 2, OnubPBP3 has Arg70 in the place of a highly conserved His70, and the C-terminus is relatively more polar because of the presence of additional charged residues. Both His70 and the C-terminus are reported to play a critical role in ligand binding and release mechanisms of these well-characterized PBPs.[18−36] Thus, these substitutions in the OnubPBP3 primary sequence may have bearing on its structure and function.

Here, we report the cloning, overexpression, refolding, and purification of OnubPBP3. The affinity of the recombinant protein toward the pheromones was determined with fluorescence binding and a competitive assay. The behavior of the protein at various pH values was characterized by high-resolution solution nuclear magnetic resonance (NMR). Homology-based modeling and molecular dynamics (MD) simulations were performed to gain insight into the protein structure, dynamics, as well as its interaction with the pheromones.

## METHODS

**Subcloning.** The OnubPBP3 gene was cloned into the pET21a vector (Novagen/EMD Millipore). Briefly, the following two primers were utilized to amplify OnubPBP3 gene from the template using the polymerase chain reaction (PCR): forward, 5′-GGAATTCCATATGTCACAAACAGTGATGAGA-3′; and reverse: 5′-GCGGATCCTCACGAATTCCACATATCGGACAC-3′ (restriction sites underlined). The amplified and purified PCR product was digested with NdeI and BamHI restriction enzymes and was inserted in pET21a vector precisely between NdeI and BamHI sites. Finally, the orientation and sequence of the OnubPBP3 gene in the pET21a vector (pET21-OnubPBP3) were confirmed through DNA sequencing.

**Expression of OnubPBP3.** The pET21-OnubPBP3 plasmid was transformed into the Origami, SHuffle, and Origami 2 competent *Escherichia coli* cell lines to determine the optimal host for recombinant protein expression. We have previously cloned ApolPBP1 in the pET21 vector and successfully expressed in Origami cells.[22] However, we were unsuccessful in expressing pET21-OnubPBP3 in Origami cells under various conditions such as temperature (30−37 °C), media (Lysogeny broth and Terrific broth), isopropyl β-D-1-thiogalactopyranoside (IPTG) concentration (0.1−1 mM), and duration of induction (4−8 h). Our efforts to express recombinant OnubPBP3 in SHuffle cells were unsuccessful as well. By contrast, Origami 2 cells[37] did express OnubPBP3, but only

```
OnubPBP3    SQTVMREMTRNFIKAYEVCAKEYNLPEATGSELINFWKEGHELTTREAGCAILCMSTKLN 60
BmorPBP     SQEVMKNLSLNFGKALDECKKEMTLTDAINEDFYNFWKEGYEIKNRETGCAIMCLSTKLN 60
ApolPBP1    SPEIMKNLSNNFGKAMDQCKDELSLPDSVVADLYNFWKDDYVMTDRLAGCAINCLATKLD 60
AtraPBP1    SPEIMKDLSINFGKALDTCKKELDLPDSINEDFYKFWKEDYEITNRLTGCAIKCLSEKLE 60
LdisPBP2    SKDVMHQMALKFGKPIKLCQQELGADDSVVKEFLDFWKDGYVMKDRQTGCMLICMAMKLE 60
            *  :*:::: :* *  . * .*    ::   :: .***:.: :. * :** : *:: **:

OnubPBP3    LLDVQGSVHRGNTVEFAKHHGSDDAMAHQVVDILHACEKAT-P--NEDKCMLALSIAMCF 117
BmorPBP     MLDPEGNLHHGNAMEFAKKHGADETMAQQLIDIVHGCEKSTPA--NDDKCIWTLGVATCF 118
ApolPBP1    VVDPDGNLHHGNAKDFAMKHGADETMAQQLVDIIHGCEKSAPP--NDDKCMKTIDVAMCF 118
AtraPBP1    MVDADGKLHHGNAREFAMKHGADDAMAKQLVDLIHGCEKSIPP--NDDRCMEVLSIAMCF 118
LdisPBP2    LLDSAMEIHHGSTFAFAKAHGADEAMAQQIIDIVHGCTTTYPAAETNDPCQRAVNVAMCF 120
            ::*   .:*:*.:  **  **:*::**:*::*::*.* .:     .:* *  .:.:* **

OnubPBP3    KAEIHKLDWAPNHELMFEELVSDMWNS  144
BmorPBP     KAEIHKLNWAPSMDVAVGEILAEV---  142
ApolPBP1    KKEIHKLNWVPNMDLVIGEVLAEV---  142
AtraPBP1    KKEIHNLKWAPNMEVVVGEVLAEV---  142
LdisPBP2    KADVHKLNWAPDVELLVADFLAESQ--  145
            * ::*:*.*.*. :: . :.:::
```

**Figure 2.** Sequence alignment of different PBPs of moths: *Ostrinia nubilalis* (GenBank Accession Number (Acc. Num.) GU828021), *Bombyx mori* (Acc. Num. X94987), *Antheraea polyphemus* (Acc. Num. X17559), *Amyelois transitella* (Acc. Num. GQ433364), *Lymantria dispar* (Acc. Num. AF007858). Two biological gates: His70 (Arg70 in case of OnubPBP3) and His95, and the C-terminus are highlighted in red color. C-terminus residues that are charged are shown in white. Conserved cysteine residues are in red and highlighted in yellow. Conserved sequence is identified with (*), conservative substitution with (:), semiconservative substitution with (.), and nonconservative substitution with ( ).


https://doi.org/10.1021/acs.jafc.1c03775
J. Agric. Food Chem. XXXX, XXX, XXX−XXX

as inclusion bodies, despite efforts at optimizing temperature, IPTG concentration, and duration of induction. Briefly, saturated overnight LB-ampicillin bacterial culture was diluted (1:70, v/v) in LB medium to express unlabeled OnubPBP3. Fresh LB-ampicillin bacterial culture was grown at 37 °C with shaking. The cell density was monitored with a UV/visible spectrophotometer (Ultrospec 2100 pro). The protein expression was induced by adding 1 mM IPTG when the optical density at 600 nm ($OD_{600}$) was 0.50−0.60. The bacterial culture was grown at 30 °C for 6 h after the induction. The cells were harvested via centrifugation (Sorvall LYNX 4000 centrifuge) at 9000 rpm and 4 °C for 30 min. The $^{15}N$-labeled OnubPBP3 was expressed by diluting the saturated overnight bacterial culture (1:50 v/v) in a minimal medium containing 0.12% [$^{15}N$] ammonium chloride. The rest of the expression conditions were the same as unlabeled except the cells in minimal medium were grown for 16 h after induction with IPTG.

**Purification and Refolding of OnubPBP3.** The harvested bacterial cells were resuspended in Bacterial Protein Extraction Reagent (B-PER, Thermo-Scientific) containing 0.2 mM ethylenediaminetetraacetic acid (EDTA) and lysed by sonication (10 cycles of 5 s each with 1 min gap) followed by centrifugation at 12,000 rpm and 4 °C for 30 min. The inclusion bodies (IBs) were collected and washed two times with dilute B-PER solution with sonication. Refolding of the protein was initiated by step dialysis to obtain the active protein. Approximately 0.6 g IBs (wet weight) was solubilized in 25 mL of 50 mM Tris−HCl buffer of pH 8.0 containing 6 M Guanidine hydrochloride (GuHCl) and 10 mM DTT followed by overnight incubation at room temperature. The sample was centrifuged at 12,000 rpm and 4 °C for 30 min. The supernatant was diluted with an equal volume of 50 mM Tris−HCl containing 2 M GuHCl. The solution was dialyzed successively in buffer 1 (50 mM Tris−HCl containing 2 M GuHCl), buffer 2 (1 M GuHCl, 0.8 M arginine, 0.9 mM oxidized glutathione, and 3 mM reduced glutathione in 50 mM Tris−HCl), and buffer 3 (0.5 M GuHCl, 0.4 M arginine, 0.45 mM oxidized glutathione, and 1.5 μM reduced glutathione in 50 mM Tris−HCl). Each step was performed at 4 °C overnight. In the final step of the refolding process, the sample was collected and centrifuged to remove any precipitated particles. The clear supernatant was dialyzed in buffer 4 (50 mM Tris−HCl, 0.1 M arginine, 250 mM NaCl, 0.9 mM oxidized glutathione, and 3 mM reduced glutathione) at 4 °C overnight.

The purification of the refolded protein sample was carried out using a combination of dialysis, DEAE anion exchanger, and finally with size exclusion chromatography. Briefly, the sample in 20 mM Tris−HCl, pH 8.0 was injected into a DEAE FF 16/10 column fitted to an AKTA Pure (GE Healthcare). The eluted fractions were analyzed by SDS-PAGE. The fractions containing OnubPBP3 were pooled, concentrated, and injected into a Superdex 75 column for size exclusion chromatography (SEC). Fractions were monitored by SDS-PAGE and the pure monomeric protein was collected and stored at 4 °C for further downstream applications.

**Protein Delipidation.** OnubPBP3 was delipidated by Lipidex-1000 resin (PerkinElmer) by modifying a previously reported protocol.[20] The resin was loaded onto a column, washed thoroughly with nanopure water, and equilibrated with 50 mM sodium citrate buffer at pH 4.5 (buffer A). The pure recombinant OnubPBP3 sample was exchanged to buffer A with a Millipore ultrafiltration concentrator (capacity 15 mL, MWCO 3000). The protein sample was loaded onto the Lipidex column and incubated for 30 min at 37 °C. The protein was eluted and buffer exchanged with 15 mM sodium phosphate buffer at pH 6.5 for fluorescence binding and competitive displacement assays.

**Fluorescence Spectroscopy.** The fluorescence binding assay of OnubPBP3 was conducted with *N*-phenyl-1-naphthylamine (1-NPN), a fluorescent probe, using a PerkinElmer LS-55 fluorescence spectrometer. The sample for fluorescence measurement was prepared in 3 mL of 15 mM sodium phosphate buffer, pH 6.5, in the presence of 0.3% methanol containing 1 μM delipidated OnubPBP3 at 22 °C. A 2 mM stock solution of 1-NPN in methanol was also prepared for the titration experiment. The mixture was equilibrated for 10 min at room temperature in a quartz cuvette (1 cm light path length) before each measurement. Emission and excitation slit widths were set to 7 and 4.7 nm, respectively. The fluorescence spectra were recorded at an excitation wavelength of 337 nm and an emission wavelength of 400−600 nm. The binding of 1-NPN to delipidated OnubPBP3 was studied by monitoring the increase in the 1-NPN fluorescence at 409 nm. To the 1 μM protein solution, aliquots were added successively from 1-NPN stock solution to a final concentration of 0−25.6 μM. All experiments were performed in triplicate, and the spectra were corrected by employing proper controls. The $k_{NPN}$ value was determined using the single-site binding equation by Origin 2019 (eq 1).

$$y = B\,x/(k + x) \tag{1}$$

where $B$ is the maximum fluorescence intensity, which represents the maximum binding capacity, $k$ is the dissociation constant, $x$ is the pheromone concentration, and $y$ is the fluorescence intensity at the specific ligand concentration.

The competitive displacement assay was performed to determine the affinity of E-11-14:OAc and Z-11-14:OAc pheromones to OnubPBP3. This assay involved the displacement of 1-NPN from the OnubPBP3:1-NPN complex with each pheromone separately while monitoring the fluorescence of 1-NPN. Briefly, a solution of delipidated OnubPBP3 (2 μM) was equilibrated overnight with 2 μM 1-NPN at 4 °C in the dark. The fluorescence of 1-NPN was recorded at the same excitation and emission wavelength as for the fluorescence binding assay described above. Aliquots of pheromone were added from a 1 mM stock solution followed, by 10 min incubation before recording the spectrum. Control experiments were performed for each addition of pheromone to a 2 μM 1-NPN solution in the absence of the protein. The $IC_{50}$ values were determined using the equation below with Origin 2019 (eq 2).

$$y = 1 - x/(k + x) \tag{2}$$

where $k$ is the $IC_{50}$, $x$ is the pheromone concentration, and $y$ is the fluorescence intensity at the specific ligand concentration.

To calculate the $K_d$ of delipidated OnubPBP3 with each pheromone, the $K_{1\text{-NPN}}$ and $IC_{50}$ values were substituted in the following equation (eq 3).

$$K_d = [IC_{50}]/(1 + [1 - \text{NPN}]/K_{1-\text{NPN}}) \tag{3}$$

where [1-NPN] is the free concentration of 1-NPN and $K_{1\text{-NPN}}$ is the dissociation constant of the complex protein:1-NPN.

**NMR Experiments and Data Analysis.** NMR samples consisted of 600 μM uniformly $^{15}N$-labeled OnubPBP3 in 50 mM phosphate buffer pH 6.5 at 25 °C, 95% $H_2O$, 5% $D_2O$, 1 mM EDTA, and 0.01% (w/v) $NaN_3$ in a Shigemi tube. NMR data were collected on the Bruker Neo 600 MHz spectrometer at 35 °C at the Oklahoma Statewide Shared (OSS) NMR facility at Oklahoma State University (Stillwater). The two-dimensional-[$^1H$, $^{15}N$] heteronuclear single quantum coherence (HSQC) experiments were performed on the OnubPBP3 sample at three different pH values (6.5, 5.5, 4.5). After reaching pH 4.5, the pH was changed back to 6.5, and an HSQC experiment was performed. The pH values were adjusted using either 1 M HCl or 1 M NaOH. The collected data were processed and analyzed by NMRPipe[38] and Sparky,[39] respectively.

**Homology Modeling.** Homology-based modeling of OnubPBP3 was carried out by using the SWISS-MODEL server[40,41] to calculate the three-dimensional structure of the protein. A suitable template was determined through the Blast and HHblits searches. The BmorPBP structure at physiological pH (PDB ID: 1LS8)[32] was chosen to be the template. The selection criteria of this template were contingent upon exhibiting a high value of GMQE (Global Model Quality Estimation), high sequence identity compared with other suggested templates, and appropriate pH. The resultant OnubPBP3 model was used in MD simulations.

**MD Simulation.** The GROMACS 5.1.5 software package[42] was used to perform 100 ns MD simulations for the free protein and its complexes with either E- or Z-pheromone (E11-tetradecenyl acetate


https://doi.org/10.1021/acs.jafc.1c03775
J. Agric. Food Chem. XXXX, XXX, XXX−XXX

and Z11-tetradecenyl acetate). The Gromos54a7 force field[43] was chosen to generate a protein topology file. The topology and force-field parameters for both pheromones were generated using the Automated Topology Builder server.[44] MD simulations were carried out in a periodic cubic box where the protein alone or the protein−ligand complex was placed at least 1.0 nm from box edges. The system was solvated by adding SPC water and then neutralized by adding 9 $Na^+$ ions. The energies of the systems were minimized through the steepest descent approach. The modified Berendsen thermostat with a time constant of 1.0 ps was used to maintain the temperature of systems at 300 K. *NVT* equilibration was performed on the systems followed by *NPT* equilibration. The computations for this project were performed at the OSU High-Performance Computing Center at Oklahoma State University (OSU). The LIGPLOT[45] program was used to show the pheromone interactions with the protein. VMD software[46] was utilized to show 3D structures of free and bound OnubPBP3. The DSSP program[47,48] enabled us to follow the evolution in the secondary structure of free and bound OnubPBP3 over the entire simulation time. The GROMACS package was utilized to calculate root mean square deviation (RMSD) values for the protein and root mean square fluctuation (RMSF) values for each residue. The ΔRMSF values were calculated from the resultant RMSF of free and bound OnubPBP3.

## RESULTS

**Protein Expression, Purification, and Refolding.** The expression of OnubPBP3 was attempted in three competent *Escherichia coli* cell lines including Origami, SHuffle, and Origami 2. All strains are specifically designed for proteins containing disulfide bonds.[49,50] The Origami *E. coli* cells[49] that were used successfully for the expression of recombinant ApolPBP1[19,20] failed to express OnubPBP3. The recently engineered SHuffle[50] was similarly unsuccessful to express OnubPBP3 under various conditions. By contrast, the pET21-OnubPBP3 plasmid was successfully expressed in *E. coli* Origami 2 cells.[37] The expression conditions, including temperature, IPTG concentration, and duration of induction, were varied in an attempt to obtain soluble protein in Origami 2 cells. However, the recombinant protein was expressed as IBs under all the conditions we attempted. Thus, the aggregated protein in the IBs had to be denatured and renatured in order to obtain the native protein. In the present study, the refolding protocol was established and used for the first time to produce the native PBP. This protocol was developed by modifying a method employed for refolding human granulocyte macrophage colony-stimulating factor.[51] The unlabeled and $^{15}N$-labeled recombinant OnubPBP3 were purified by DEAE anion exchange chromatography followed by SEC on a Superdex 75 column fitted to the AKTA FPLC system. SEC and SDS-PAGE analysis revealed that the purified recombinant OnubPBP3 sample was homogeneous (Figure 3A,B).

**Pheromone Binding Affinity by Fluorescence.** 1-NPN, an extrinsic fluorescent dye, was used as an external probe to investigate the hydrophobic environment/pocket in OnubPBP3. 1-NPN exhibited a very low fluorescence intensity of 140 when 25.6 $\mu$M of 1-NPN was added to the solution without the protein. The intensity of this probe was highly amplified to 856 in the presence of OnubPBP3, indicating that the probe was bound to the hydrophobic pocket of the protein. The $\lambda_{max}$ of the 1-NPN shifted to a shorter wavelength upon binding to the protein. The normalized fluorescence intensity was plotted against the concentration of free 1-NPN to determine the dissociation constant $K_{1\text{-NPN}}$ of the OnubPBP3:1-NPN complex, which is 3.804 $\mu$M (Figure 4A).

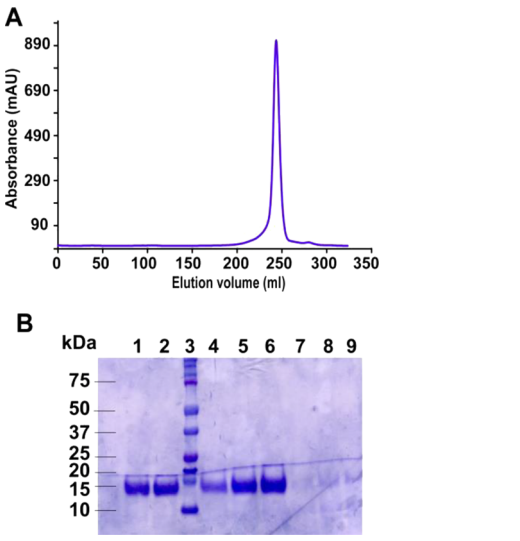


**Figure 3.** SEC and Coomassie-stained SDS-PAGE of refolded and purified OnubPBP3 (A) Size exclusion chromatogram of OnubPBP3 (B) SDS-PAGE of OnubPBP3; Lane 1,2,4,5, and 6: pure protein from different fractions after SEC; lanes 3: protein molecular weight marker; Lanes 7,8, and 9: fractions after SEC which do not have protein.

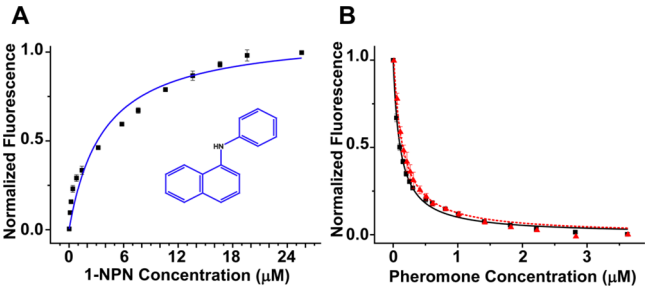


**Figure 4.** Competitive displacement assay of 1-NPN with E- and Z-pheromones of OnubPBP3. (A) Normalized fluorescence intensity as a function of 1-NPN concentration used to calculate $K_{NPN}$. OnubPBP3 (1 $\mu$M) in 15 mM phosphate buffer, pH 6.5, was titrated with increasing amounts of 1-NPN to a final concentration of 25.6 $\mu$M. Chemical structure of 1-NPN is shown in the plot. (B) Competitive displacement fluorescence binding assay [2 $\mu$M OnubPBP3 in 15 mM phosphate buffer, pH 6.5 in complex with 1-NPN (2 $\mu$M)]. Normalized maximum fluorescence emission of 1-NPN was recorded after increasing concentrations (0−3.6 $\mu$M) of E-11-14:OAc (solid black) and Z-11-14:OAc (dashed red) were added. Both plots were employed to determine $IC_{50}$ of each pheromone. Both assays were carried out in triplicate.

Fluorescence spectroscopy has been commonly used to investigate the competitive displacement of 1-NPN from a protein:1-NPN complex by a ligand in order to determine the dissociation constant of the ligand.[52−54] The binding affinity of OnubPBP3 with the two sex pheromones was investigated by performing the competitive displacement assay (Figure S1A−D). The $IC_{50}$ was calculated by plotting the normalized fluorescence intensity against the concentration of the free pheromone (Figure 4B). The $IC_{50}$ values of E-11-14:OAc and Z-11-14:OAc were 108.1, and 139.4 nM, respectively. OnubPBP3 showed a high binding affinity to both E- and Z-pheromones with $K_d$ values of 71 and 91 nM, respectively.

**Effect of pH on OnubPBP3.** The 2D-[$^1H$,$^{15}N$] HSQC spectrum was collected for $^{15}N$-labeled OnubPBP3 at pH 6.5


https://doi.org/10.1021/acs.jafc.1c03775
J. Agric. Food Chem. XXXX, XXX, XXX−XXX

(Figure 5A). This HSQC spectrum is the fingerprint region of a protein. Any change in this spectrum because of changes in

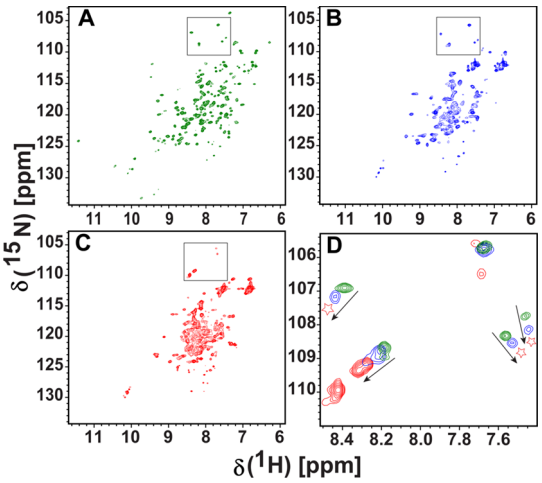


**Figure 5.** Two-dimensional [$^{1}$H, $^{15}$N] HSQC spectra obtained on 600 $\mu$M OnubPBP3 at different pH. (A) OnubPBP3 at pH 6.5. (B) OnubPBP3 at pH 5.5. (C) OnubPBP3 at pH 4.5.(D) Overlay of the expanded view of the boxed region from three spectra collected at different pH values: 6.5 in green, 5.5 in blue, and 4.5 in red; arrows indicate the direction of the chemical shift change, red stars refer to missing peaks at pH 4.5.

the protein environment, such as variation in pH, solvent, temperature, salt concentration, ligand binding, and so on, reflects a change in protein conformation. Thus, the conformational change of a protein can be observed conveniently by monitoring the HSQC spectrum under various conditions. Furthermore, HSQC is a reliable experiment to check the suitability of a protein sample for 3D structure determination. Indeed, the HSQC spectrum of refolded OnubPBP3 at pH 6.5 showed well-dispersed peaks, suggesting a well-folded protein that is suitable for structure−function studies by solution-state NMR (Figure 5A).

To test the effect of pH on OnubPBP3 conformation, HSQC spectra were collected at pH 6.5, 5.5, and 4.5. The NMR spectra showed that the peak dispersion diminished with the lowering of pH from near neutral to the acidic range (Figure 5A−D). The spectrum of the protein at pH 5.5 revealed that the reduction of the pH by one unit was enough to produce a drastic change in conformation (Figure 5B). Lowering the pH to 4.5 showed a dramatic effect, with most of the peaks collapsing to the center of the HSQC (Figure 5C). Indeed, many peaks were missing from their original position in the spectrum of the protein at pH 6.5 (Figure 5A). These peaks moved to the center of the spectrum at pH 4.5 (Figure 5C). This collapse is an indication of pH-induced unfolding of the protein. Figure 5D is an overlay of the expanded view of a region from three spectra collected at different pH values. This region had fewer peaks that are quite isolated to effectively show the pH effect on the protein structure. To test whether OnubPBP3 was irreversibly denatured at pH 4.5, the pH was increased back to 6.5. Interestingly, the HSQC, collected after this pH increase, matched the original HSQC spectrum very well (Figure S2), suggesting that this pH-induced effect is reversible.

**Homology Model of OnubPBP3 and MD.** The three-dimensional model of OnubPBP3 was constructed through homology-based modeling since the high-resolution structure is not available. Homology modeling requires a candidate template structure which exists in the protein data bank. The quality of the predicted model by this method relies on the degree of protein-sequence similarity and identity between the studied protein and the template. The higher the identity or similarity between both proteins at the sequence level, the higher the reliability of the predicted structure. However, a sequence identity of at least 30% is necessary for homology modeling to work.[55] The sequence of OnubPBP3 and the selected template are 86.6% similar and 52.8% identical, suggesting that the predicted model is reliable. Furthermore, distribution of the amino acid Phi and Psi angles in the constructed model shows 87.77% of the residues are in the

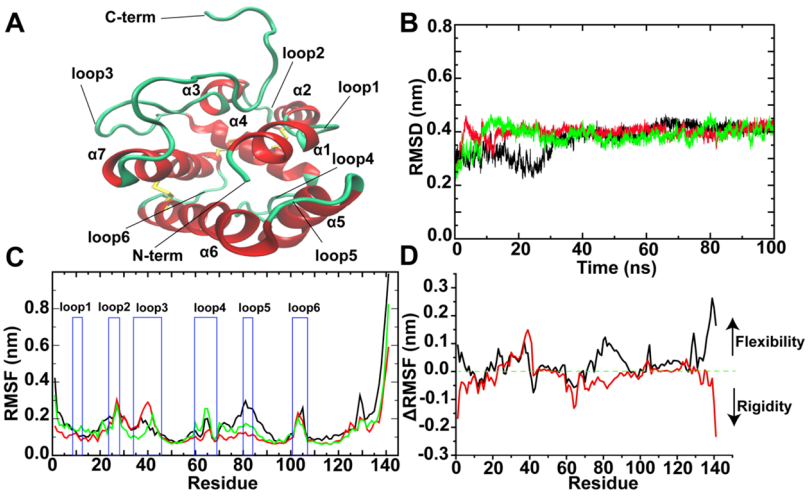


**Figure 6.** (A) Homology-based model of OnubPBP3 (image was generated with VMD[39] software). $\alpha$-Helices, loops, and termini are labeled and the disulfide bonds are shown in yellow color. In the 100 ns MD simulations shown in (B), (C) and (D), free OnubPBP3 is shown in green, OnubPBP3 bound to E-pheromone in red, OnubPBP3 bound to Z-pheromone in black. (B) Backbone atom RMSD calculated for free and bound OnubPBP3. (C) C$\alpha$-RMSF calculated for free and bound OnubPBP3; all loop areas in the plots were pointed via rectangles and labeled as in the homology model. (D) Differences between RMSF plots of free and bound OnubPBP3. Direction of the increase in flexibility and rigidity is shown by black arrows.


https://doi.org/10.1021/acs.jafc.1c03775
J. Agric. Food Chem. XXXX, XXX, XXX−XXX

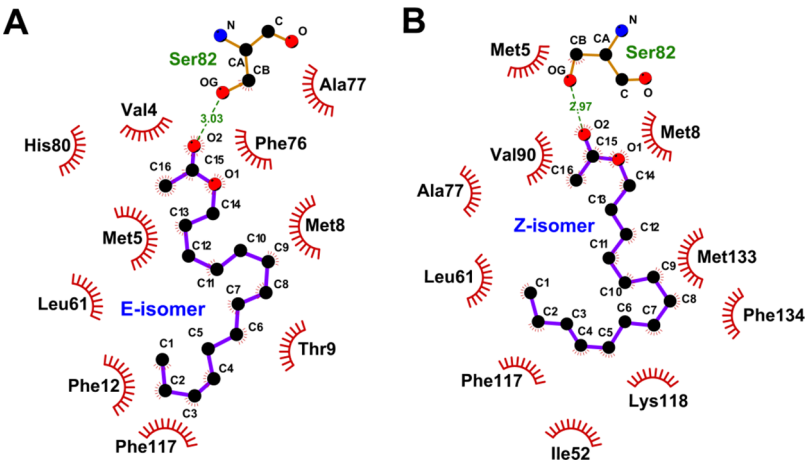


**Figure 7.** LIGPLOT diagram illustrating the interactions between pheromones and OnubPBP3 in each complex. Interactions of OnubPBP3 with (A) E-11-14:OAc and (B) Z-11-14:OAc where hydrogen bond is represented by green dashed line with indicated distances (in Å) and hydrophobic interaction is displayed as arcs with spokes radiating toward the pheromone molecule. Atoms are color coded (carbon, black; oxygen, red; nitrogen, blue).

most favored regions, indicating the high quality of the model. The model consists of seven $\alpha$-helices: Thr3-Met8 ($\alpha$1), Ile13-Tyr23 ($\alpha$2), Ala28-Leu33 ($\alpha$3), Glu47-Leu59 ($\alpha$4), Arg70-His80 ($\alpha$5), Asp84-Ala100 ($\alpha$6), and Cys107-Leu124 ($\alpha$7). Six loops connect the helices in this model: Thr9-Phe12 (loop1), Asn24-Glu27 (loop2), Ile34-Arg46 (loop3), Asn60-His69 (loop4), Gly81-Asp83 (loop5), and Thr101-Lys106 (loop6). The C-terminus (Asp125-Ser144) does not have any characteristic structural features and is exposed to the solvent (Figure 6A). Moreover, three disulfide bonds were formed between cysteine residues, Cys19-Cys54, Cys50-Cys107, and Cys97-Cys116, connecting $\alpha$2 to $\alpha$4, $\alpha$4 to $\alpha$7, and $\alpha$6 to $\alpha$7, respectively. The three disulfide bonds stabilize the hydrophobic pocket as well as the overall protein structure.

MD simulations were conducted to gain insight into the binding of OnubPBP3 with E- or Z-pheromones to compare and contrast their binding interactions and protein dynamics upon binding. Individual MD simulations of 100 ns were performed on the free OnubPBP3 and its corresponding complexes with the E- and Z-pheromones. To remove the bias from the placement and orientation of ligand into the OnubPBP3 binding pocket, MD simulations were performed by placing the E-ligand at four different location in the protein (Figure S3). Regardless of the starting position, the ligand entered the hydrophobic binding pocket at the end of each MD simulation (Figure S3).

The RMSD is used to measure global protein flexibility and stability. RMSDs of backbone atoms of free and bound OnubPBP3 were calculated (Figure 6B). The RMSD of the OnubPBP3:E-pheromone complex converged at 13 ns with an average value of 0.40 nm. However, the OnubPBP3:Z-pheromone complex reached equilibrium at 32 ns with an average RMSD value of 0.40 nm. RMSD of free OnubPBP3 with an average value of 0.39 nm showed relatively more fluctuation than both the complexes. The free OnubPBP3 reached the maximum stability at 10 ns but had some fluctuation (relative to the complexes) throughout the 100 ns simulation.

The RMSF of each residue in a protein is used to determine the residue-specific flexibility. The C$\alpha$-RMSFs for the three simulations were calculated over the 100 ns trajectories and averaged over each individual residue in the protein (Figure 6C). The differences in the flexibility of various segments of the OnubPBP3:E/Z-pheromone complex have been provided in Table S1 in the Supporting Information. Briefly, the RMSF of free OnubPBP3 showed very high fluctuations at both termini (Figure 6C, green trace), indicating high flexibility. As expected, the following loop regions: Tyr23-Thr29, Phe36-Thr45, Leu59-Val68, Gly71-Asp92, and Thr101-Lys106, were more flexible than the structured regions. The RMSF of the free protein and the OnubPBP3:E-pheromone complex exhibited similar fluctuations in the following loop regions, Tyr23-Thr29 and Thr101-Lys106. However, Leu59-Val68, Gly71-Asp92 as well as the termini showed less flexibility, while Gly30-Thr45 exhibited higher flexibility for this complex. The RMSF of the OnuBPB3:Z-pheromone complex showed increased flexibility compared to the free protein at both termini and the following loop regions: Ile34-Glu39, Gly71-Asp92, and Thr101-Lys106. However, flexibility decreased at Gly40-Leu43 and Leu59-Val68. The difference of the RMSF ($\Delta$RMSF) of each residue between the free protein and each complex offers a better representation of flexibility variations (Figure 6D). The $\Delta$RMSF of the protein:E-pheromone complex showed an increase in rigidity in 61% of the residues of the protein in the complex. In contrast, $\Delta$RMSF of the protein:Z-pheromone complex exhibited an increase in the flexibility in 75% of the protein residues as a result of binding.

Analysis of both complexes after the simulations revealed the amino acid residues that interact with the ligands. The E-pheromone formed hydrophobic interactions with Val4, Met5, Met8, Thr9, Phe12, Leu61, Phe76, Ala77, His80, and Phe117. It also formed a hydrogen bond (3.03 Å) with Ser82 (Figure 7A). The Z-pheromone formed a hydrogen bond to Ser82 (Figure 7B), with a slightly shorter length (2.97 Å). Like the E-pheromone, the Z-pheromone showed hydrophobic interactions with Met5, Met8, Leu61, and Ala77. However, it also showed hydrophobic interactions with Phe11, Met33, Ile52, Leu61, Ala77, Lys118, Met133, and Phe134 (Figure 7A,B).

Since the E- and Z-pheromones have different interactions with OnubPBP3, we monitored the secondary structural changes induced by the pheromones during MD simulations. The homology model lost its first $\alpha$-helix (Thr3-Met8) after 2 ns of the MD simulation (Figure 8A), resulting in an unstructured N-terminus (Ser1-Phe12) with the first $\alpha$-helix


https://doi.org/10.1021/acs.jafc.1c03775
J. Agric. Food Chem. XXXX, XXX, XXX−XXX

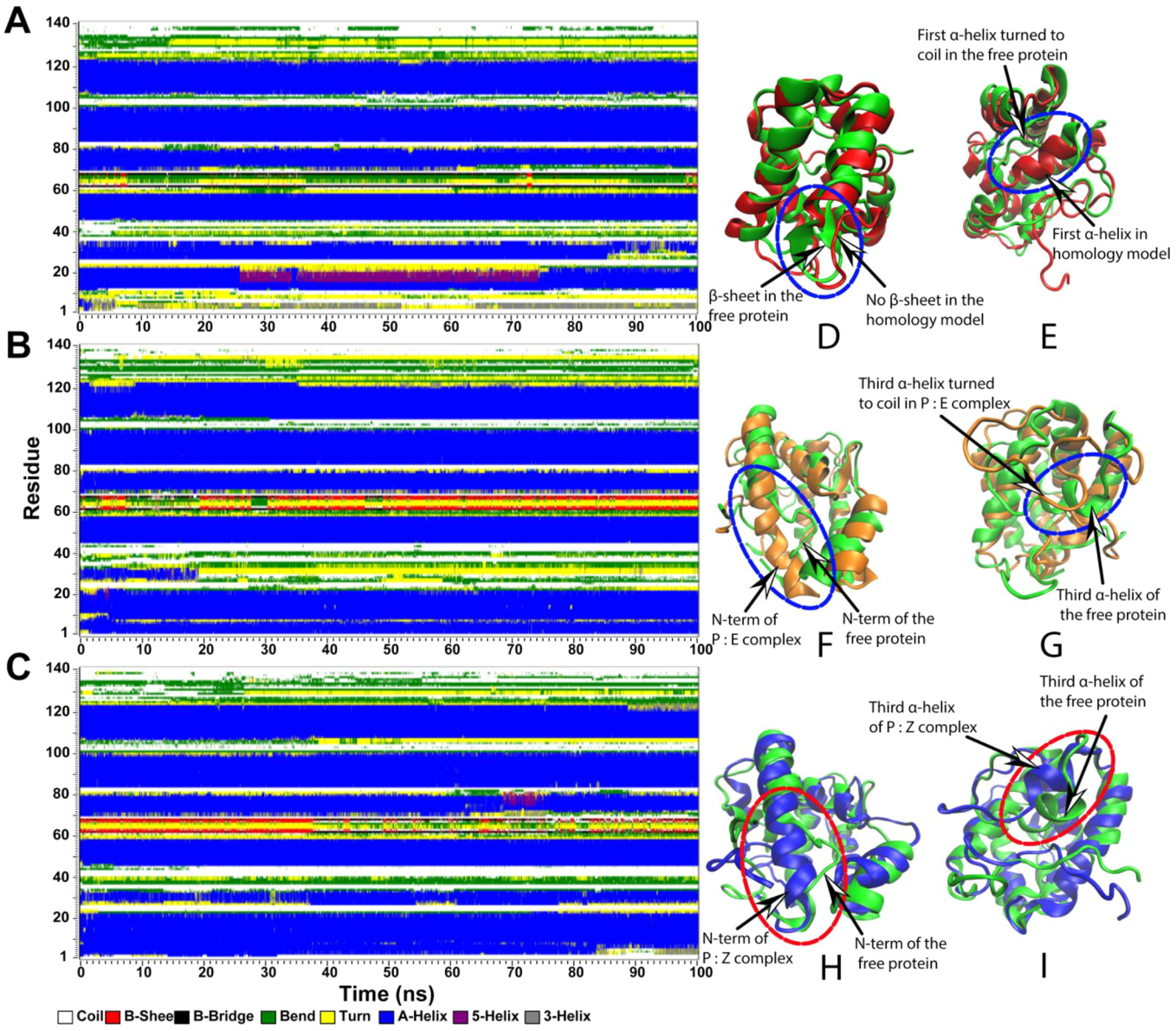


**Figure 8.** Structural analyses of OnubPBP3 in three 100 ns trajectories. On the left, secondary structures as a function of time for the protein as calculated by DSSP program: (A) the free protein, (B) the protein bound to the E-pheromone, (C) the protein bound to the Z-pheromone. On the right, comparison of the structures after 100 ns MD simulations (these images were generated with VMD[39] software): (D) and (E), the initial homology-based model in red is overlaid with a snapshot at 100 ns of the free protein in green; the regions showing significant structural change are encircled in blue, loop4 in D and the first $\alpha$-helix in E; (F) and (G), structures of free (green) and bound OnubPBP3 to E-pheromone (orange) are overlaid. Significant structural change is encircled in blue, the N-terminus in F and the third $\alpha$-helix in G; (H) and (I), structures of free (green) and bound OnubPBP3 to Z-pheromone (blue) are overlaid. Regions showing significant structural change are encircled in red, the N-terminus in H and the third $\alpha$-helix in I.

starting at residue Ile13 in the free protein (Figure 8E). However, the first $\alpha$-helix started at residue Gln2 in the E-pheromone complex (Figure 8B,F) and at residue Arg6 in the Z-pheromone complex (Figure 8C,H). Secondary structure analysis of free OnubPBP3 and its Z-pheromone complex showed that the Gly30-Asn35 and Glu27-Leu33 segments, respectively, as $\alpha$-helices (Figure 8I). However, the Asn24-Thr45 segment in the bound OnubPBP3 with E-pheromone was completely unstructured (Figure 8G). Moreover, the simulation of the free protein showed a transient antiparallel $\beta$-sheet between the Leu62-Asp63 and Ser67-Val68 beta-strands that was absent in the homology model (Figure 8A,D). This $\beta$-sheet structure is stabilized upon binding to the E-pheromone (Figure 8B,C).

## DISCUSSION

Although OnubPBP3 shares over 50% sequence identity with several well-studied lepidopteran PBPs including ApolPBP1,[18−24] AtraPBP1,[25,26] BmorPBP,[27−34] and LdisPBPs[35,36](Figure 2), there are critical differences in two biological gates (highlighted in red in Figure 2). The histidine gate is composed of His70 and His85 for these PBPs[18−36] (Figure 2), however, in OnubPBP3, His70 is replaced by Arg70 (Figure 2). Furthermore, the C-terminal gate (Pro128-Ser144) in OnubPBP3 is more polar than these PBPs[18−36]-36(Figure 2). Similar differences have been reported in the primary structure of *Ostrinia furnacalis* pheromone binding protein2 (OfurPBP2).[56] These critical differences in the


https://doi.org/10.1021/acs.jafc.1c03775
J. Agric. Food Chem. XXXX, XXX, XXX−XXX

primary structure of OnubPBP3 may have an impact on its tertiary structure and consequently on its function. Thus, a detailed characterization of OnubPBP3 is necessary to understand the mechanism of pheromone communication in *Ostrinia nubilalis* if the control of this invasive pest through pheromone inhibition to be achieved. However, there is no report on recombinant expression or characterization of any PBP from *O. nubilalis*. This is the first report on overexpression, purification, and structural characterization of a PBP from *O. nubilalis*. We have cloned, overexpressed, and produced pure and homogeneous OnubPBP3 for a detailed characterization of this protein through biochemical, biophysical, and computational approaches. Understanding the structural mechanisms of pheromone binding and release in this species may help in the design of pheromone mimetics for integrated pest management.

The OnubPBP3 gene was cloned and overexpressed in bacteria after optimization of various conditions. The recombinant protein was successfully refolded from IBs using a stepwise dialysis protocol and purified to homogeneity using a combination of dialysis, anion exchange, and size exclusion chromatograph techniques. The proper folding of the recombinant OnubPBP3 and its affinity toward the pheromone isomers were investigated through its ability to bind 1-NPN and both the ligands using a fluorescence-based assay technique. 1-NPN fluoresces weakly in aqueous environments, but its fluorescence increases dramatically in a hydrophobic environment. 1-NPN has been utilized routinely to determine the folding, and binding affinities of PBPs to their respective ligands.[19−21,56,57] In the present study, the titration of 1-NPN to OnubPBP3 resulted in a large increase in fluorescence intensity with a distinct blue shift of the emission maximum. The dissociation constant of 1-NPN ($K_{1\text{-NPN}}$) was determined to be 3.804 $\mu$M (Figure 4A).

The 1-NPN fluorescence in the protein:1-NPN complex at pH 6.5 quenched remarkably in the competitive displacement assay with each of the pheromones. OnubPBP3 did bind both E- and Z-pheromone with high affinity with a $K_d$ of 71 and 91 nM, respectively (Figure 4B). Our competitive binding assay data demonstrated that the recombinant OnubPBP3 is folded properly and exists in the pheromone binding form at pH 6.5. This observation was further validated with the quality of the 2D-HSQC NMR spectrum at pH 6.5 (Figure 5A). The HSQC spectrum, collected under suitable biological conditions, is considered the fingerprint of a protein. The quality of this spectrum in terms of dispersion of resonances can indicate whether the protein under study is well-folded or in a molten globule or denatured state. The HSQC data collected on $^{15}$N-labeled OnubPBP3 at pH 6.5 in 50 mM phosphate buffer showed good dispersion of resonances suggesting that the recombinant OnubPBP3 is well-folded and is suitable for further biophysical characterization.

Several lepidopteran moth PBPs including, ApolPBP1,[18−24] AtraPBP1,[25,26] BmorPBP,[28] and LdisPBPs,[35,36] have been reported to bind ligand above pH 6.0 and release it at a lower pH of 4.5 while undergoing a pH-dependent conformational switch. These proteins have two unique conformations, open (or bound or PBP$^B$) and closed (or free or PBP$^A$). Switching between these two conformations relies on the pH of the solution and the presence/absence of a ligand. Bound PBPs at neutral pH adopt the open conformation, where the C-terminus is unstructured and flexible, extending out to the solvent,[33] On the other hand, the free PBPs are in the closed conformation in which the C-terminus becomes an $\alpha$-helix and occupies the hydrophobic cavity. The ligand binding at higher pH (above 6.0) and release at lower pH (below 5.0) are controlled by two biological gates, His70 and His95 at one end of the binding pocket, and the C-terminus at the other end. In the ligand-bound conformation at higher pH, the histidine gate is closed while the C-terminal gate is opened with the unstructured C-terminus exposed to the solvent. However, at acidic pH near the olfactory receptor neuron, the histidine gate is opened due to charge repulsion between the protonated histidines while the C-terminal gate is closed by the newly formed C-terminal $\alpha$-helix that occupies the binding pocket pushing the ligand out through the other end of the pocket (histidine gate).[18−36]

To investigate the effect of pH on the OnubPBP3 conformation, pH titration studies were carried out using NMR. HSQC spectra were collected at pH 6.5, 5.5, and finally at 4.5. As the pH was lowered, the peak dispersion decreased with increased crowding at the center of the HSQC spectra (Figure 5A−D). An expanded view of the boxed region from the overlay of three spectra demonstrated the change in the chemical shifts with the change in pH (Figure 5D). Evidently, OnubPBP3 undergoes a drastic conformational transition to what appears to be a partially unfolded state or molten globule state when the pH is lowered to 4.5. This behavior of OnubPBP3 with changing pH is quite similar to the behavior of OfurPBP2 that we have reported recently.[56] The secondary structure of OfurPBP2[56] in far-UV CD (180−250 nm) region was not affected significantly by changing pH from pH 6.5 to pH 4.5. OnubPBP3 showed a very similar behavior in far-UV CD (data not shown). Both proteins maintain helical structure at pH 4.5 although their tertiary structure /conformation is affected as seen in the 2D HSQC. The fact that the protein's secondary structure is retained but its tertiary structure/fold is affected suggests that it is likely in a molten globule state. To investigate the reversibility of this conformational transition, the pH was restored to 6.5 and an HSQC spectrum was collected. Overlaying the initial and the final HSQC spectra recorded at pH 6.5 demonstrated that the conformational transition is reversible (Figure S2), similar to what has been reported for OfurPBP2.[56]

Although OnubPBP3 undergoes a pH-dependent conformational transition similar to other well-investigated lepidopteran PBPs, it behaves very differently at low pH. Unlike ApolPBP1, BmorPBP, and AtraPBP1, which have a well-defined low-pH conformation, OnubPBP3 does not appear to have a clear low-pH conformation. These differences suggest that OnubPBP3 may have a distinct mechanism of ligand release.

A thorough MD investigation of free and bound OnubPBP3 was conducted to map the binding surface and to gain an understanding of the amino acid residues involved in the interaction with the pheromone. MD simulations showed that both E- and Z-pheromones interact primarily through hydrophobic interactions with the protein. However, not all the interactions with the protein are the same for these two pheromones. Both E- and Z-isomers interact with Met5, Met8, Leu61, Ala77, and Ser82. In addition, the E-isomer specifically interacts with Val4, Thr9, Phe12, Phe76, His80, and Phe117, while the Z-isomer interacts specifically with Phe11, Met33, Ile52, Lys118, Met133, and Phe134. Each system (i.e., free protein and each complex) reached equilibrium at a different time in the simulation (Figure 6B). However, free OnubPBP3 exhibited slight conformational divergence after 10 ns until the


https://doi.org/10.1021/acs.jafc.1c03775
J. Agric. Food Chem. XXXX, XXX, XXX−XXX

end of the simulation. Upon binding to either pheromone, the stability of the protein increased, as indicated by the RMSD values (Figure 6B). To gain insight into protein dynamics upon ligand binding, RMSF values of free and bound proteins were calculated. Analysis of the protein fluctuations revealed the loops joining the $\alpha$-helices and both termini were most flexible for the free protein (Figure 6A,C). Most of the flexible segments of the free protein became relatively rigid upon binding to E-pheromone while the opposite effect was observed with Z-pheromone for some of the segments. The differences in the protein dynamics between the two complexes are shown by ΔRMSF (Figure 6D). The ΔRMSF values indicate the Z-pheromone binding increased the protein dynamics in contrast to the E-pheromone. Often a protein becomes less disordered upon binding to its ligand.[58] In other words, a higher affinity ligand will stabilize a protein more than a ligand with a lower affinity. The $K_d$ values determined by competitive displacement assay were 71 nM for the E-isomer and 91 nM for the Z-isomer. Taken together, the binding constants and ΔRMSF indicate the E-pheromone forms a more stable complex with OnubPBP3 than Z-pheromone.

Analysis of the evolution of the secondary structure of the free protein and both complexes throughout the MD simulations demonstrates that there are subtle changes in OnubPBP3 conformation upon binding to each ligand. In particular, the N-terminus exhibited some differences in each case. For the OnubPBP3:E-pheromone complex, while the $\alpha$3-helix disappeared, the antiparallel $\beta$-sheet became more prominent. For the OnubPBP3:Z-pheromone complex, the $\alpha$3-helix showed some differences in the residues content compared to that of free protein. In addition, the antiparallel $\beta$-sheet became more noticeable relative to the free protein.

A thorough understanding of the structure and function of proteins involved in olfaction are necessary to achieve biorational control of invasive pests such as *O. nubilalis*. This is the first report of recombinant expression and functional studies through ligand binding assays by fluorescence and NMR on OnubPBP3. Our study not only provides important insight into the structure of OnubPBP3, but also provides a framework for future investigations to understand the mechanism of pheromone recognition, binding, and release in this invasive agricultural pest.

## ■ ASSOCIATED CONTENT

### Supporting Information

The Supporting Information is available free of charge at https://pubs.acs.org/doi/10.1021/acs.jafc.1c03775.

Fluorescence spectra for binding assay, NMR spectra, and MD simulations of the OnubPBP3:E-pheromone complex (PDF)

## ■ AUTHOR INFORMATION


### Corresponding Author

**Smita Mohanty** − *Department of Chemistry, Oklahoma State University, Stillwater, Oklahoma 74078, United States;* orcid.org/0000-0002-1680-6338; Email: smita.mohanty@okstate.edu

### Authors

**Omar Al-Danoon** − *Department of Chemistry, Oklahoma State University, Stillwater, Oklahoma 74078, United States*

**Suman Mazumder** − *Department of Chemistry, Oklahoma State University, Stillwater, Oklahoma 74078, United States*

**Bharat P. Chaudhary** − *Department of Chemistry, Oklahoma State University, Stillwater, Oklahoma 74078, United States*

**Viswanath Nukala** − *Department of Chemistry, Oklahoma State University, Stillwater, Oklahoma 74078, United States*

**Benton Bishop** − *Department of Chemistry, Oklahoma State University, Stillwater, Oklahoma 74078, United States*

**Gage Cahoon** − *Department of Chemistry, Oklahoma State University, Stillwater, Oklahoma 74078, United States*

Complete contact information is available at: https://pubs.acs.org/10.1021/acs.jafc.1c03775


### Author Contributions

S. Mohanty conceived and designed the strategies employed, developed the delipidation technique, supervised the research, and analyzed the data; S.M. designed the primers and cloned the gene; B.B. and G.C. optimized protein expression, B.B. optimized protein refolding, O.A. performed protein expression, further optimization of refolding, purification, and delipidation, prepared samples, collected NMR and fluorescence data, processed the data, and performed MD simulations; B.C. performed some of the MD simulations, VN performed some of the data analysis, S.M. and O.A. wrote the paper; and O.A. and B.C. prepared figures.


### Funding

Funding for this project was provided by the U.S. Department of Agriculture NIFA Award # 2011-65503-23501, NSF Award CHE-1807722, NSF MRI Award DBI-1726397, and NSF REU Award CHE-1559874 to S. Mohanty.


### Notes

The authors declare no competing financial interest.

## ■ ACKNOWLEDGMENTS

We thank Dr. Thomas Webb of Auburn University and Dr. Darrell Berlin of Oklahoma State University for critical reading and Jacob Lewellen for proofreading of the manuscript.

## ■ REFERENCES


(1) Vogt, R. G.; Riddiford, L. M., *Pheromone reception: a kinetic equilibrium in mechanisms in insect olfaction*; Clarendon Press; Oxford University Press: Oxford [Oxfordshire]; New York, 1986.

(2) Leal, W. S. Odorant reception in insects: roles of receptors, binding proteins, and degrading enzymes. *Annu. Rev. Entomol.* **2013**, *58*, 373−391.

(3) Brito, N. F.; Moreira, M. F.; Melo, A. C. A. A look inside odorant-binding proteins in insect chemoreception. *J. Insect Physiol.* **2016**, *95*, 51−65.

(4) Ishida, Y.; Leal, W. S. Rapid inactivation of a moth pheromone. *Proc. Natl. Acad. Sci. U. S. A.* **2005**, *102*, 14075.

(5) Hutchison, W. D.; Burkness, E. C.; Mitchell, P. D.; Moon, R. D.; Leslie, T. W.; Fleischer, S. J.; Abrahamson, M.; Hamilton, K. L.; Steffey, K. L.; Gray, M. E.; Hellmich, R. L.; Kaster, L. V.; Hunt, T. E.; Wright, R. J.; Pecinovsky, K.; Rabaey, T. L.; Flood, B. R.; Raun, E. S. Areawide Suppression of European Corn Borer with Bt Maize Reaps Savings to Non-Bt Maize Growers. *Science* **2010**, *330*, 222.

(6) Bohnenblust, E. W.; Breining, J. A.; Shaffer, J. A.; Fleischer, S. J.; Roth, G. W.; Tooker, J. F. Current European corn borer, Ostrinia nubilalis, injury levels in the northeastern United States and the value of Bt field corn. *Pest Manage. Sci.* **2014**, *70*, 1711−1719.

(7) Frolov, A. N.; Bourguet, D.; Ponsard, S. Reconsidering the taxomony of several Ostrinia species in the light of reproductive isolation: a tale for Ernst Mayr. *Biol. J. Linn. Soc.* **2007**, *91*, 49−72.

(8) Hansson, B. S.; Löfstedt, C.; Roelofs, W. L. Inheritance of olfactory response to sex pheromone components in Ostrinia nubilalis. *Naturwissenschaften* **1987**, *74*, 497−499.
(9) Kochansky, J.; Cardé, R. T.; Liebherr, J.; Roelofs, W. L. Sex pheromone of the European corn borer, Ostrinia nubilalis (Lepidoptera: Pyralidae), in New York. *J. Chem. Ecol.* **1975**, *1*, 225−231.
(10) Ishikawa, Y.; Takanashi, T.; Kim, C.-G.; Hoshizaki, S.; Tatsuki, S.; Huang, Y. Ostrinia spp. in Japan: their host plants and sex pheromones. *Entomol. Exp. Appl.* **1999**, *91*, 237−244.
(11) Cardé, R. T.; Roelofs, W. L.; Harrison, R. G.; Vawter, A. T.; Brussard, P. F.; Mutuura, A.; Munroe, E. European Corn Borer: Pheromone Polymorphism or Sibling Species? *Science* **1978**, *199*, 555−556.
(12) Linn, C., Jr.; O'Connor, M.; Roelofs, W. Silent genes and rare males: a fresh look at pheromone blend response specificity in the European corn borer moth. Ostrinia nubilalis. *J. Insect Sci.* **2003**, *3*, 15.
(13) Klun, J. A.; Chapman, O. L.; Mattes, K. C.; Wojtkowski, P. W.; Beroza, M.; Sonnet, P. E. Insect Sex Pheromones: Minor Amount of Opposite Geometrical Isomer Critical to Attraction. *Science* **1973**, *181*, 661.
(14) Anglade, P.; Stockel, J.; I.W.G.O. Cooperators. Intraspecific sex-pheromone variability in the European corn borer, Ostrinia nubilalis Hbn.(Lepidoptera, Pyralidae). *Agronomie* **1984**, *4*, 183−187.
(15) Willett, C. S.; Harrison, R. G. Pheromone binding proteins in the European and Asian corn borers: no protein change associated with pheromone differences. *Insect Biochem. Mol. Biol.* **1999**, *29*, 277−284.
(16) Willett, C. S.; Harrison, R. G. Insights Into Genome Differentiation: Pheromone-Binding Protein Variation and Population History in the European Corn Borer (Ostrinia nubilalis). *Genetics* **1999**, *153*, 1743.
(17) Allen, J. E.; Wanner, K. W. Asian corn borer pheromone binding protein 3, a candidate for evolving specificity to the 12-tetradecenyl acetate sex pheromone. *Insect Biochem. Mol. Biol.* **2011**, *41*, 141−149.
(18) Damberger, F. F.; Ishida, Y.; Leal, W. S.; Wüthrich, K. Structural basis of ligand binding and release in insect pheromone-binding proteins: NMR structure of Antheraea polyphemus PBP1 at pH 4.5. *J. Mol. Biol.* **2007**, *373*, 811−819.
(19) Katre, U. V.; Mazumder, S.; Mohanty, S. Structural insights into the ligand binding and releasing mechanism of Antheraea polyphemus pheromone-binding protein 1: role of the C-terminal tail. *Biochemistry* **2013**, *52*, 1037−1044.
(20) Katre, U. V.; Mazumder, S.; Prusti, R. K.; Mohanty, S. Ligand Binding Turns Moth Pheromone-binding Protein into a pH Sensor: EFFECT ON THE ANTHERAEA POLYPHEMUS PBP1 CONFORMATION. *J. Biol. Chem.* **2009**, *284*, 32167−32177.
(21) Mazumder, S.; Chaudhary, B. P.; Dahal, S. R.; Al-Danoon, O.; Mohanty, S. Pheromone Perception: Mechanism of the Reversible Coil-Helix Transition in Antheraea polyphemus Pheromone-Binding Protein 1. *Biochemistry* **2019**, *58*, 4530−4542.
(22) Mohanty, S.; Zubkov, S.; Gronenborn, A. M. The solution NMR structure of Antheraea polyphemus PBP provides new insight into pheromone recognition by pheromone-binding proteins. *J. Mol. Biol.* **2004**, *337*, 443−451.
(23) Mohanty, S.; Ring, J.; Prusti, R. Chemical Communication: A Visit with Insects. *Curr. Chem. Biol.* **2008**, *2*, 83−96.
(24) Zubkov, S.; Gronenborn, A. M.; Byeon, I. J.; Mohanty, S. Structural consequences of the pH-induced conformational switch in A.polyphemus pheromone-binding protein: mechanisms of ligand release. *J. Mol. Biol.* **2005**, *354*, 1081−1090.
(25) Leal, W. S.; Ishida, Y.; Pelletier, J.; Xu, W.; Rayo, J.; Xu, X.; Ames, J. B. Olfactory proteins mediating chemical communication in the navel orangeworm moth, Amyelois transitella. *PLoS One* **2009**, *4*, No. e7235.
(26) Xu, W.; Xu, X.; Leal, W. S.; Ames, J. B. Extrusion of the C-terminal helix in navel orangeworm moth pheromone-binding protein (AtraPBP1) controls pheromone binding. *Biochem. Biophys. Res. Commun.* **2011**, *404*, 335−338.
(27) Damberger, F.; Horst, R.; Wüthrich, K.; Peng, G.; Nikonova, L.; Leal, W. S. NMR characterization of a pH-dependent equilibrium between two folded solution conformations of the pheromone-binding protein from Bombyx mori. *Protein Sci.* **2000**, *9*, 1038−1041.
(28) Damberger, F. F.; Michel, E.; Ishida, Y.; Leal, W. S.; Wuthrich, K. Pheromone discrimination by a pH-tuned polymorphism of the Bombyx mori pheromone-binding protein. *Proc. Natl. Acad. Sci. U. S. A.* **2013**, *110*, 18680−18685.
(29) di Luccio, E.; Ishida, Y.; Leal, W. S.; Wilson, D. K. Crystallographic Observation of pH-Induced Conformational Changes in the Amyelois transitella Pheromone-Binding Protein AtraPBP1. *PLoS One* **2013**, *8*, No. e53840.
(30) Horst, R.; Damberger, F.; Luginbuhl, P.; Guntert, P.; Peng, G.; Nikonova, L.; Leal, W. S.; Wuthrich, K. NMR structure reveals intramolecular regulation mechanism for pheromone binding and release. *Proc. Natl. Acad. Sci. U. S. A.* **2001**, *98*, 14374−14379.
(31) Lautenschlager, C.; Leal, W. S.; Clardy, J. Coil-to-helix transition and ligand release of Bombyx mori pheromone-binding protein. *Biochem. Biophys. Res. Commun.* **2005**, *335*, 1044−1050.
(32) Lee, D.; Damberger, F. F.; Peng, G.; Horst, R.; Güntert, P.; Nikonova, L.; Leal, W. S.; Wüthrich, K. NMR structure of the unliganded Bombyx mori pheromone-binding protein at physiological pH. *FEBS Lett.* **2002**, *531*, 314−318.
(33) Sandler, B. H.; Nikonova, L.; Leal, W. S.; Clardy, J. Sexual attraction in the silkworm moth: structure of the pheromone-binding-protein-bombykol complex. *Chem. Biol.* **2000**, *7*, 143−151.
(34) Xu, W.; Leal, W. S. Molecular switches for pheromone release from a moth pheromone-binding protein. *Biochem. Biophys. Res. Commun.* **2008**, *372*, 559−564.
(35) Kowcun, A.; Honson, N.; Plettner, E. Olfaction in the gypsy moth, Lymantria dispar: effect of pH, ionic strength, and reductants on pheromone transport by pheromone-binding proteins. *J. Biol. Chem.* **2001**, *276*, 44770−44776.
(36) Terrado, M.; Okon, M.; McIntosh, L. P.; Plettner, E. Ligand- and pH-Induced Structural Transition of Gypsy Moth Lymantria dispar Pheromone-Binding Protein 1 (LdisPBP1). *Biochemistry* **2020**, *59*, 3411−3426.
(37) Long, X.; Gou, Y.; Luo, M.; Zhang, S.; Zhang, H.; Bai, L.; Wu, S.; He, Q.; Chen, K.; Huang, A.; Zhou, J.; Wang, D. Soluble expression, purification, and characterization of active recombinant human tissue plasminogen activator by auto-induction in E. coli. *BMC Biotechnol.* **2015**, *15*, 13.
(38) Delaglio, F.; Grzesiek, S.; Vuister, G. W.; Zhu, G.; Pfeifer, J.; Bax, A. NMRPipe: a multidimensional spectral processing system based on UNIX pipes. *J. Biomol. NMR* **1995**, *6*, 277−293.
(39) Lee, W.; Tonelli, M.; Markley, J. L. NMRFAM-SPARKY: enhanced software for biomolecular NMR spectroscopy. *Bioinformatics* **2015**, *31*, 1325−1327.
(40) Waterhouse, A.; Bertoni, M.; Bienert, S.; Studer, G.; Tauriello, G.; Gumienny, R.; Heer, F. T.; de Beer, T. A. P.; Rempfer, C.; Bordoli, L.; Lepore, R.; Schwede, T. SWISS-MODEL: homology modelling of protein structures and complexes. *Nucleic Acids Res.* **2018**, *46*, W296−W303.
(41) Bienert, S.; Waterhouse, A.; de Beer, T. A. P.; Tauriello, G.; Studer, G.; Bordoli, L.; Schwede, T. The SWISS-MODEL Repository—new features and functionality. *Nucleic Acids Res.* **2017**, *45*, D313−D319.
(42) Berendsen, H. J. C.; van der Spoel, D.; van Drunen, R. GROMACS: A message-passing parallel molecular dynamics implementation. *Comput. Phys. Commun.* **1995**, *91*, 43−56.
(43) Schmid, N.; Eichenberger, A. P.; Choutko, A.; Riniker, S.; Winger, M.; Mark, A. E.; van Gunsteren, W. F. Definition and testing of the GROMOS force-field versions 54A7 and 54B7. *Eur. Biophys. J.* **2011**, *40*, 843.
(44) Malde, A. K.; Zuo, L.; Breeze, M.; Stroet, M.; Poger, D.; Nair, P. C.; Oostenbrink, C.; Mark, A. E. An Automated Force Field


https://doi.org/10.1021/acs.jafc.1c03775
J. Agric. Food Chem. XXXX, XXX, XXX−XXX

Topology Builder (ATB) and Repository: Version 1.0. *J. Chem. Theory Comput.* **2011**, *7*, 4026−4037.
(45) Wallace, A. C.; Laskowski, R. A.; Thornton, J. M. LIGPLOT: a program to generate schematic diagrams of protein-ligand interactions. *Protein Eng. Des. Sel.* **1995**, *8*, 127−134.
(46) Humphrey, W.; Dalke, A.; Schulten, K. VMD: Visual molecular dynamics. *J. Mol. Graph.* **1996**, *14*, 33−38.
(47) Joosten, R. P.; te Beek, T. A. H.; Krieger, E.; Hekkelman, M. L.; Hooft, R. W. W.; Schneider, R.; Sander, C.; Vriend, G. A series of PDB related databases for everyday needs. *Nucleic Acids Res.* **2011**, *39*, D411−D419.
(48) Kabsch, W.; Sander, C. Dictionary of protein secondary structure: Pattern recognition of hydrogen-bonded and geometrical features. *Biopolymers* **1983**, *22*, 2577−2637.
(49) Xiong, S.; Wang, Y.-F.; Ren, X.-R.; Li, B.; Zhang, M.-Y.; Luo, Y.; Zhang, L.; Xie, Q.-L.; Su, K.-Y. Solubility of disulfide-bonded proteins in the cytoplasm of Escherichia coli and its ″oxidizing″ mutant. *World J. Gastroenterol.* **2005**, *11*, 1077−1082.
(50) Lobstein, J.; Emrich, C. A.; Jeans, C.; Faulkner, M.; Riggs, P.; Berkmen, M. SHuffle, a novel Escherichia coli protein expression strain capable of correctly folding disulfide bonded proteins in its cytoplasm. *Microb. Cell Fact.* **2012**, *11*, 753.
(51) Thomson, C. A.; Olson, M.; Jackson, L. M.; Schrader, J. W. A simplified method for the efficient refolding and purification of recombinant human GM-CSF. *PLoS One* **2012**, *7*, No. e49891.
(52) Zhou, J.-J.; Zhang, G.-A.; Huang, W.; Birkett, M. A.; Field, L. M.; Pickett, J. A.; Pelosi, P. Revisiting the odorant-binding protein LUSH of Drosophila melanogaster: evidence for odour recognition and discrimination. *FEBS Lett.* **2004**, *558*, 23−26.
(53) Siciliano, P.; He, X. L.; Woodcock, C.; Pickett, J. A.; Field, L. M.; Birkett, M. A.; Kalinova, B.; Gomulski, L. M.; Scolari, F.; Gasperi, G.; Malacrida, A. R.; Zhou, J. J. Identification of pheromone components and their binding affinity to the odorant binding protein CcapOBP83a-2 of the Mediterranean fruit fly, Ceratitis capitata. *Insect Biochem. Mol. Biol.* **2014**, *48*, 51−62.
(54) Waris, M. I.; Younas, A.; ul Qamar, M. T.; Hao, L.; Ameen, A.; Ali, S.; Abdelnabby, H. E.; Zeng, F.-F.; Wang, M.-Q. Silencing of Chemosensory Protein Gene NlugCSP8 by RNAi Induces Declining Behavioral Responses of Nilaparvata lugens. *Front. Physiol.* **2018**, *9*, 379.
(55) Fiser, A. Template-based protein structure modeling. *Methods Mol. Biol.* **2010**, *673*, 73−94.
(56) Mazumder, S.; Dahal, S. R.; Chaudhary, B. P.; Mohanty, S. Structure and Function Studies of Asian Corn Borer Ostrinia furnacalis Pheromone Binding Protein2. *Sci. Rep.* **2018**, *8*, 17105−17105.
(57) Zhang, T.; Sun, Y.; Wanner, K. W.; Coates, B. S.; He, K.; Wang, Z. Binding affinity of five PBPs to Ostrinia sex pheromones. *BMC Mol. Biol.* **2017**, *18*, 4.
(58) Nguyen, D. D.; Xiao, T.; Wang, M.; Wei, G.-W. Rigidity Strengthening: A Mechanism for Protein−Ligand Binding. *J. Chem. Inf. Model.* **2017**, *57*, 1715−1721.


https://doi.org/10.1021/acs.jafc.1c03775
*J. Agric. Food Chem.* XXXX, XXX, XXX−XXX